THE JOURNAL OF PHYSICAL CHEMISTRY A

pubs.acs.org/JPCA Article

Computational Comparative Analysis of Small Atomically Precise Copper Clusters

Adebola Adeagbo, Tao Wei, and Andre Z. Clayborne*

Cite This: J. Phys. Chem. A 2020, 124, 6504–6510 Read Online

ACCESS | Metrics & More | Article Recommendations | Supporting Information

ABSTRACT: Atomically precise copper clusters (APC) have attracted attention for their promise in sensing, water remediation, and electrochemical technologies. However, smaller-sized APCs and the evolution of their properties as a function of size and composition are not clearly understood. Here, we have performed an investigation into the electronic structure, geometry, and optical properties of small atomically precise copper clusters using density functional theory (DFT) and time-dependent DFT. Through comparative analysis, we show that the electronic structures of the experimentally characterized clusters, $Cu_4(PN(C_6H_5)_2CH)_4$ and $Cu_4(SN_2C_7H_{11})_4$, are similar with the closed-shell superatom character $1S^21P^2$. By changing the ligand on $Cu_4(PN(C_6H_5)_2CH)_4$ and $Cu_4(SN_2C_7H_{11})_4$, there were no major changes observed in the tetrahedral Cu_4 core geometry, electronic structure, or optical spectra. However, a change in the anchor atom causes an increase in the electronic gap and induces a hypochromic shift in the onset peak in the optical spectrum of the small clusters. Increasing the copper core size showed small changes Cu−Cu bond lengths, lower electronic gap values, and a bathochromic shift in the optical spectra. Computational results not only provide detailed physical insight into APCs but also aid in identifying compound compositions of small atomically precise nanoclusters from data collected in the experiment.

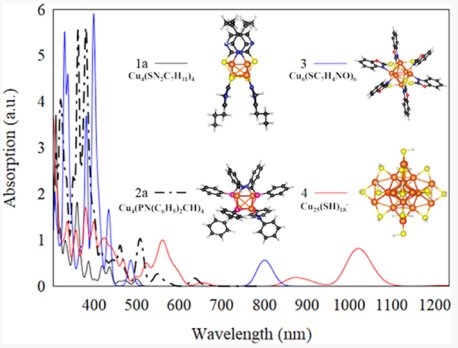

1. INTRODUCTION

From the size of their metal cores to their organic ligands, atomically precise nanoparticles offer the tailor ability needed to achieve desired electronic and optical properties. Of particular interest, many studies have focused on atomically precise ligated nanoparticles of gold and silver. The biocompatibility, tunability, and wide range of applications for sensing, drug delivery, and catalysis have excited researchers for decades.[1−6]

Similar to gold and silver, atomically precise copper nanoparticles have experienced a renewed interest for researchers. Copper has significant biological and industrial importance and is more affordable than gold and silver, which has sparked researchers to pursue a better understanding of these nanoparticles. Though copper nanoparticles exhibit a sensitivity to the surrounding environment that can lead to difficulty in their characterization,[7] recent years have shown that these can be overcome and showed promises in catalytic, optoelectronic, and sensing technologies.[8−11] For example, ligated Cu catalysts have successfully converted CO_2 to formic acid. Wang et al.[12] illustrated that copper can reduce methylene blue dye. Gao and co-workers[7] showed that $Cu_6(SC_7H_4NO)_6^-$ could be used for the electrochemical detection of H_2O_2. Tang and co-workers illustrated using experiment and density functional theory (DFT) that the electrochemical reduction of CO_2 occurs on the ligated copper nanoparticle via a lattice-hydride mechanism.

In other works, researchers have strived to understand the geometry and stability of Cu nanoparticles. For example, Kacprzak et al.[13] used DFT calculations to theoretically characterize cyclic thiolated copper clusters. Nanoparticles such as $Cu_{13}\{S_2CN_nBu_2\}_6(acetylide)_4^+$ and $[Cu_{61}(S^tBu)_{26}S_6Cl_6H_{14}]^+$ have been described as superatoms, which rely on the delocalization of metallic states over the nanoparticle core.[11,14] However, the thiolated copper-hydride nanocluster $Cu_{25}H_{10}(SPhCl_2)_{18}^{3-}$ lacks superatom states, but it is reported to be stable due to atom-ligand interactions.[15] In a more recent study, Han and co-workers synthesized an atomically precise copper cluster that incorporates a neutral tetrahedral copper core.[16] Interestingly, while researchers have focused on larger atomically precise Cu_n nanoparticles (i.e., $n > 8$), smaller-sized ligated copper nanoclusters are often neglected theoretically though synthesized readily. A detailed study of smaller-sized atomically precise copper clusters (APCs) could provide key structural and electronic information as a starting point to understand the formation of larger APCs. These details could lay the foundation toward determining the preferential copper core size or geometry to be used in nanoscale devices with varying applications.

Received: May 4, 2020
Revised: June 29, 2020
Published: July 21, 2020

https://dx.doi.org/10.1021/acs.jpca.0c03992
J. Phys. Chem. A 2020, 124, 6504–6510

Herein, our purpose is to gain insight into the structural, electronic, and optical properties of small atomically precise ligated copper clusters (i.e., $Cu_4(SN_2C_7H_{11})_4$ and $Cu_4(PN(C_9H_{11})_2CH)_4$). We not only probe the intricacies of their fundamental properties using DFT and time-dependent DFT but also explore how these properties evolve due to ligand composition and anchor atom choice. These results are compared to those obtained through UV−vis experiments. Further, we address the progression of optical response properties through changes in copper core size. To the best of our knowledge, there are no computational studies that address how the properties of atomically precise copper clusters, sometimes referred to as ligated superatom clusters, change due to the number of copper atoms in the core.

2. COMPUTATIONAL METHODS

The calculations in this work were performed using density functional theory (DFT) as implemented in the GPAW[17−19] code at the PBE[20] level. Geometry optimizations were performed with a grid spacing of 0.2 and 7.0 Å of vacuum surrounding each nanoparticle system. In each simulation, all atoms were allowed to move freely without constraints until the forces on all atoms were below a threshold of 0.05 eV/Å. In previous studies by our group and others, we have found this method produces results within a reasonable amount of error for gold and copper nanoparticle systems.[7]

Initial geometries for $Cu_4(SN_2C_7H_{11})_4$[21] (**1a**), $Cu_4(PN(C_9H_{11})_2CH)_4$,[22] and $Cu_6(SC_7H_4NO)_6^-$[7] were obtained from previous experimental reports. Prior to geometry optimization, we reduced the mesitylene group in the ligand of $Cu_4(PN(C_9H_{11})_2CH)_4$[22] to phenyl groups to obtain $Cu_4(PN(C_6H_5)_2CH)_4$ (**2a**). Additionally, the R-groups in the ligands of **1a** and **2a** were further reduced to methyl/hydrogen groups to obtain $Cu_4(SN_2C_3H_7)_4$ (**1b**), $Cu_4(SN_2CH_3)_4$ (**1c**), $Cu_4(PN(CH_3)_2CH)_4$ (**2b**), and $Cu_4(PNH_2CH)_4$ (**2c**). We obtained $Cu_4(SNH_2CH)_4$ (**2d**) by replacing the phosphorus atom in **2c** with a sulfur atom. Similarly, we performed geometry optimization on the neutral $Cu_6(SC_7H_4NO)_6^-$ system (**3**). Though the $Cu_6(SC_7H_4NO)_6$ system is found in the experiment as an anion, we chose to compare closed-shell systems. Though the $Cu_{25}(SH)_{18}^-$ (**4**) nanoparticle has not been synthesized, we replaced the gold atoms of the $Au_{25}(SH)_{18}^-$[23] structure from previous studies with copper atoms. All nanoparticle systems were allowed to relax as explained above.

Once all systems were in their lowest ground state, we performed analyses on their electronic structure and optical properties. A Bader analysis was performed to determine the charge on each atom. The spectra of each nanoparticle were determined using the linear response time-dependent DFT (Lr-TDDFT)[24] module as implemented in GPAW. The oscillator strengths were obtained and tabulated for the most prominent transitions for each cluster through the Lr-TDDFT module. Spectra were rendered through gnuplot.

3. RESULTS AND DISCUSSION

3.1. Geometry. Figure 1 shows the structures of the Cu_4 ligated clusters. The average bond lengths of their core copper atoms are presented in Table 1. The copper cores in all structures are tetrahedral or tetrahedral-like (Figure 1). The average Cu−Cu bond lengths of the relaxed $Cu_4(SN_2C_7H_{11})_4$ (**1a**) is 2.70 Å, which is within 0.02 Å of the experimental value. The $Cu_4(PN(C_6H_5)_2CH)_4$ (**2a**) system has the largest Cu−Cu bond length at 3.00 Å that agrees well with the experimental value. While our results agree with experimental structures, we wanted to understand the role of the ligand and anchor atom on the geometry to understand the possible observable effects on the geometry. Therefore, we altered the R-group and anchor atom of the ligand.

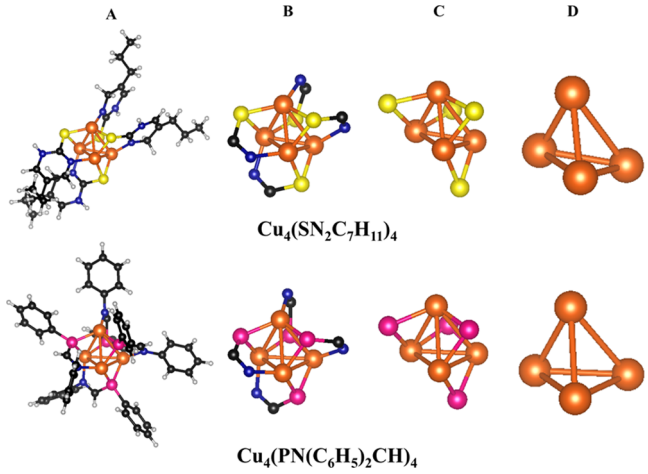

Figure 1. Comparison of Cu_4 nanocluster structures. (A) Total structures of Cu_4 nanoclusters. (B, C) Cu_4 metal cores with their bridging anchor atoms. (D) Isolated metal cores of Cu_4 nanoclusters. Legend: orange sphere, Cu; pink sphere, P; yellow sphere, S; blue sphere, N; red sphere, O; black sphere, C; and gray sphere, H.

The geometric changes to the core accompanied by changing the R-group of the ligands provide some insight into the importance of the ligand choice and effect on the core. First, we reduced the R-group on each ligand (Figure S7). For the $Cu_4(SN_2C_7H_{11})_4$ system, reducing the R-group from C_7H_{11} to C_3H_7 decreased the core bond lengths by 0.37%. By reducing it further to $Cu_4(SN_2CH_3)_4$, Cu bonds increased by 1.12% as compared to the $Cu_4(SN_2C_3H_7)_4$ system. The R-group reduction of $Cu_4(PN(C_6H_5)_2CH)_4$ to $Cu_4(PN(CH_3)_2CH)_4$ decreased the core Cu bond lengths by 0.05 Å, resulting in a 1.67% decrease. Further reducing it to $Cu_4(PNH_2CH)_4$ increased the core Cu bond lengths by 0.11 Å, resulting in a 3.73% increase. The noticeable increase by reducing the ligand to CH_3 results from the reduced steric effect of the ligand. Upon closer investigation of the core, by reducing the ligand to CH_3, the core reduces/increases the distortion in the core. This illustrates the importance of the ligand interaction and the steric effect of the ligand on the core geometry. Interestingly, the changes in core metal−metal distances observed here are similar to those observed in previous studies on thiolated gold nanoparticles.[25]

In addition to investigating the effect of reducing the R-group, we changed the anchor atom of the ligand to observe any change in geometry. The anchor atom is defined as the atom bridging the metal core to the ligand similar to our previous study.[25] To further investigate this observation, an anchor atom change was performed on the $Cu_4(PNH_2CH)_4$ system. Changing the anchor atom to a sulfur atom resulted in a 0.40 Å decrease in the average core bond lengths. The resulting $Cu_4(SNH_2CH)_4$ system has an average core bond length of 2.66 Å, which is within 0.04 Å of the **1a** system. Therefore, the anchor atom has a significant influence on the geometry of these copper systems.

Figure 2 shows the structures of Cu_6 and Cu_{25} systems, and their average bond lengths are presented in Table 2. Though both the Cu_6 and Cu_{25} nanoparticles have been studied

https://dx.doi.org/10.1021/acs.jpca.0c03992
J. Phys. Chem. A 2020, 124, 6504−6510

Table 1. Average Relaxed and Experimental Core Copper to Copper Atom, Copper to Anchor Atom, Copper to Nitrogen, Sulfur to Carbon, Phosphorus to Carbon, and Nitrogen to Carbon Atom Bond Lengths (Å) of the Cu_4 Systems in This Study and Experimental Crystal Structures

system	Cu−Cu	Cu−X_A	Cu−N	S−C	P−C	N−C
$Cu_4(SN_2C_7H_{11})_4$ (**1a**)	2.70	2.27	2.00	1.77	n/a	1.39
$Cu_4(SN_2C_3H_7)_4$ (**1b**)	2.69	2.27	2.02	1.79	n/a	1.40
$Cu_4(SN_2CH_3)_4$ (**1c**)	2.72	2.27	1.99	1.78	n/a	1.34
$Cu_4(PN(C_6H_5)_2CH)_4$ (**2a**)	3.00	2.27	2.01	n/a	1.81	1.37
$Cu_4(PN(CH_3)_2CH)_4$ (**2b**)	2.95	2.26	2.00	n/a	1.82	1.38
$Cu_4(PNH_2CH)_4$ (**2c**)	3.06	2.27	2.01	n/a	1.79	1.30
$Cu_4(SNH_2CH)_4$ (**2d**)	2.66	2.30	1.98	1.74	n/a	1.30
Expt. values[21] (**1**)	2.72	2.27	1.99	1.77	n/a	1.38
Expt. values[22] (**2**)	3.00	2.27	2.01	n/a	1.81	1.37

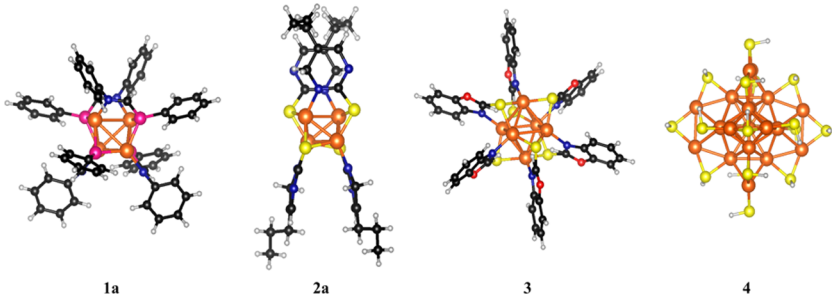

Figure 2. Ball and stick representation of all ligated copper systems in this study: **1a** ($Cu_4(SN_2C_7H_{11})_4$), **2a** ($Cu_4(PN(C_6H_5)_2CH)_4$), **3** ($Cu_6(SC_7H_4NO)_6$), and **4** ($Cu_{25}(SH)_{18}^-$). Legend: orange sphere, Cu; pink sphere, P; yellow sphere, S; blue sphere, N; red sphere, O; black sphere, C; and gray sphere, H.

Table 2. Average Bond Lengths (Å) of Cu_6 and Cu_{25} Systems

system	Cu−Cu	Cu−X_A	Cu−N	X_A−C	N−C
$Cu_6(SC_7H_4NO)_6$ (**3**)	2.83	2.27	2.05	1.73	1.36
$Cu_{25}(SH)_{18}^-$ (**4**)	2.62	2.24	n/a	n/a	n/a
Expt. values[26] (**3**)	2.64	2.38	2.07	1.71	1.36

previously, we provide their results for comparison to the smaller copper clusters.[7,21] The average Cu−Cu bond lengths of $Cu_6(SC_7H_4NO)_6$ is 2.83 Å. The average bond length here is larger than the previously calculated bond lengths and 7.20% larger than the experimental crystal structure. The source of the discrepancy may be attributed to the charge differences of the cluster. In the previous study, the cluster was negatively charged; here, the cluster is neutral.[7] The Cu_6 core still retains an octahedral polyhedron with eight faces. The bonding interaction of the ligand is similar to the Cu_4 systems with interactions through the nitrogen, carbon, and sulfur atoms. The $Cu_{25}(SH)_{18}^-$ system has the smallest average Cu−Cu bond length at 2.62 Å. While this structure is theoretical, it has a geometry similar to that of the $Au_{25}(SH)_{18}^-$ cluster with an icosahedral core.[25]

Comparing the geometries of the systems here, we note a few significant similarities and differences. While the number of copper atoms increases, the bond lengths of the average Cu−Cu bond do fluctuate only slightly ranging from 2.62 to 2.83 Å. These remain slightly larger than those observed in bulk copper surfaces (2.556 Å). It is interesting that the sulfur-containing species tend to have slightly smaller Cu−Cu bond lengths than its phosphorus counterparts. Yet, there are no noticeable effects on the Cu−S, Cu−P, or Cu−N bond lengths as the size of the copper core increases. The shortest Cu−Cu bonds are observed in the Cu_{25} structure (2.62 Å), which may be attributed to the different bonding situation of the ligands. In Cu_{25}, it has a staple motif typically observed in atomically precise gold nanoclusters, which binds only through the sulfur atom. The bonding interactions are different than other nanoclusters studied here because there are two ligand interactions with the copper cores, that is, the nitrogen and either the sulfur or phosphorus atom.

3.2. Electronic Structure. The gap between the highest occupied molecular orbital (HOMO) and the lowest unoccupied molecular orbital (LUMO), the HOMO−LUMO gap (HL gap), was determined for each of the cluster systems (Table 3). The smallest sized copper clusters (i.e., Cu_4R_4) exhibit the largest gap sizes with $Cu_4(SR)_4$ clusters having the largest HL gaps. Both **1b** and **1c** have the largest gap sizes of 2.44 eV, whereas **1a** is smaller by 0.15 eV. The phosphorus-containing clusters **2a**, **2b**, and **2c** have lower gaps than each of the sulfur-containing species with gap sizes of 1.75, 1.85, and 2.02 eV, respectively. Though the change in R-group alters the gap incrementally, when changing the phosphorus to a sulfur atom in **2**, the HL gap increases by 0.32 eV.

Table 3. HOMO−LUMO Gaps (eV) of the Ligated Copper Clusters in This Work

system	HOMO−LUMO gap (eV)
1a	2.29
1b	2.44
1c	2.44
2a	1.75
2b	1.85
2c	2.02
2d	2.34
3	1.37
4	0.94

https://dx.doi.org/10.1021/acs.jpca.0c03992
J. Phys. Chem. A 2020, 124, 6504−6510

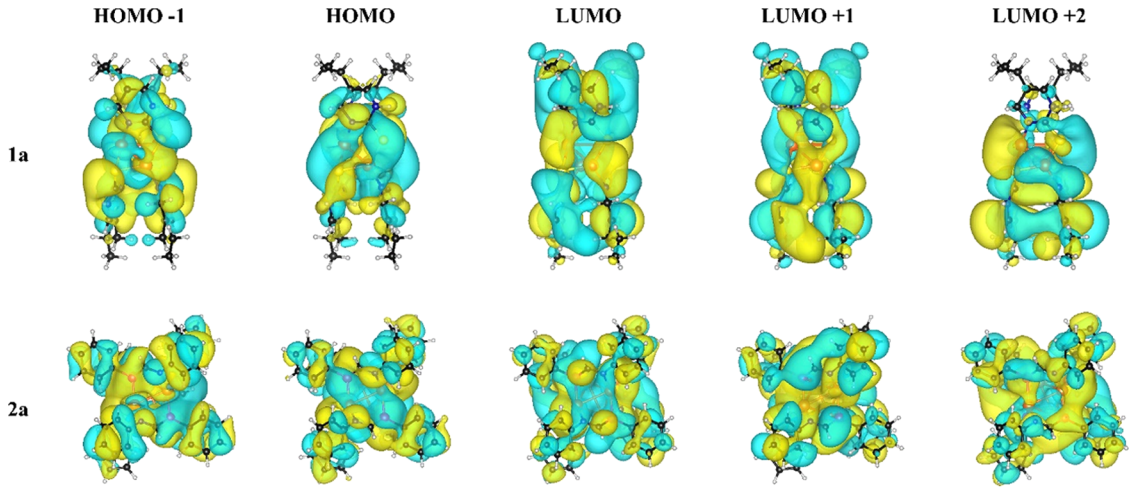

Figure 3. Representation of the HOMO and LUMO (HOMO − 1, HOMO, LUMO, LUMO + 1, LUMO + 2) states for the **1a** and **2a** systems.

As the number of copper atoms in the core increases, there is a decrease in the HL gap. Contrary to all other nanoclusters, the Cu_{25} nanocluster is the only system with a gap of less than 1 eV. Comparing Cu_6 to **1a** and **2a**, its 1.37 eV value is smaller than both fully ligated counterparts. This trend follows closely to those observed in atomically precise gold nanoparticles, where the gap decreases as the size of the system increases toward bulk materials.

In many atomically precise clusters, the electronic structure can provide insight into the stable nature of the system. Often, atomically precise nanoclusters such as gold and silver (and others) can be explained via the superatom (or superatom complex) model.[5,27−30] This model relies on the electrons of the core being iterant on the metal core. When ligands are involved, these ligands can be either electron withdrawing or electron donating. The resultant electron count can result in magic numbers that are indicative of increased stability. For many ligated copper systems, the superatom analogy can be hit or miss. Often, it is highly dependent on the oxidation state of the copper atom. To determine the possibility of **1a** and **2a** being superatoms, we investigated the Kohn−Sham orbitals and Hirschfield charge analysis.[31]

Figure 3 shows the electron density of the HOMO − 1, HOMO, LUMO, and LUMO + 1 states for the **1a** and **2a**. While the electron density is delocalized on the core, it is actually delocalized across the entire nanocluster structure (core and ligand). One may expect this if the ligands withdraw electrons from the cluster core, creating a zero-valent superatom. However, performing a Hirschfield charge analysis indicates that there is no loss of charge from the copper atoms within the core. This is similar to the findings of the tetrahedral core of the Cu_{23} nanocluster system.[16] On the other hand, this indicates the possibility of having a shell closing of $1s^21p^2$ in the superatom view.[28] A close view of the Kohn−Sham orbitals reveals that the two highest occupied molecular orbitals have *P*-symmetry occupied on the core. However, there is a significant amount of the electron density spread along the ligands (Figure 3; Supporting Information).

3.3. Optical Properties. Despite having the same number of core copper atoms, the effects of the contrasting geometries and HL gaps of the ligated Cu_4 clusters manifest themselves in the spectroscopic profile. The overall spectroscopic profiles **1a**, **1b**, and **1c** are similar with minimal differences (Figure 4a). Between 400 and 550 nm, there are five peaks observed for 1a (Figure 4).

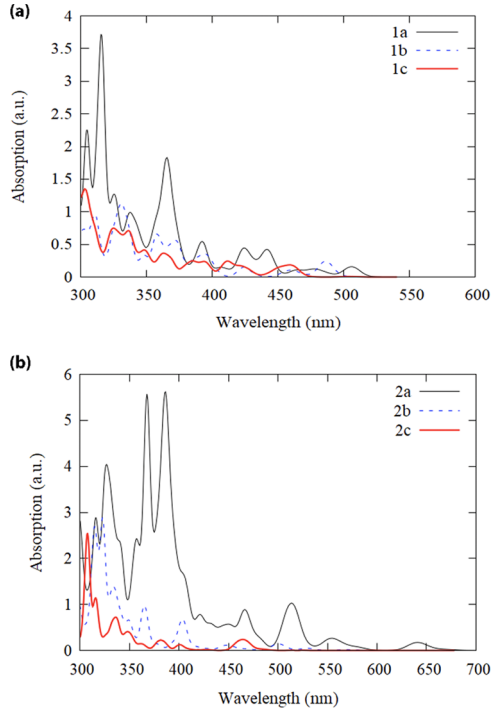

Figure 4. Theoretical UV−vis spectra of (a) **1a**, **1b**, and **1c** and (b) **2a**, **2b**, and **2c**.

These peaks correspond to transitions between HOMO and LUMO + 1 (2.45 eV), HOMO − 2 and LUMO (2.60 eV), HOMO − 3 and LUMO (2.66 eV), HOMO − 2 and LUMO + 3 (2.81 eV), and HOMO and LUMO + 5 (2.93 eV). The intense peaks observed between 300 and 400 nm have strong oscillator strengths. These transitions are from the copper core (mostly) to states where the density resides either solely on the ligand or is delocalized across the entire cluster system. Once the ligand is reduced (i.e., **1b** and **1c**), the first absorption peak observed exhibits a blue shift, first from 506 (2.450 eV) to 486 nm (2.550 eV). The peak further blue shifts to 471 nm (2.635 eV) as the R-group is further reduced (Figure 4). This is not the only effect due to the ligand reduction. In 1a, there are intense peaks observed at 370 and 380 nm. However, these are less intense in **1b** and **1c**.

https://dx.doi.org/10.1021/acs.jpca.0c03992
J. Phys. Chem. A 2020, 124, 6504−6510

The optical spectra for **2a**, **2b**, and **2c** are in Figure 4b. The first observed peak at 641 nm is a result of a transition from the HOMO to LUMO + 1. Between 500 and 600 nm, there are two peaks observed for 1a. These transitions are from the HOMO − 3 to LUMO + 2 (516 nm) and HOMO − 2 to LUMO + 1 (552 nm), respectively. Between 400 and 500 nm there are three observed peaks corresponding to transitions from the HOMO to LUMO + 6 (467 nm), HOMO − 1 to LUMO + 6 (421 nm), and HOMO − 5 to LUMO + 3 (405 nm). Similar to 1a, the peaks between 300 and 400 nm have strong oscillator strengths. All of the transitions originate and end in states where the electron density is delocalized across the entire cluster. When the system is reduced to **1b** and **1c**, the first observed peaks exhibit a blue shift. The first peak of **1b** exhibits a blue shift from 641 to 570 nm. Likewise, the first peak of **1c** exhibits a blue shift from 570 to 520 nm.

By changing the anchor atom, i.e., phosphorous (**2c**, $Cu_4(PNH_2CH)_4$) to sulfur (**2d**, $Cu_4(SNH_2CH)_4$), there are various noticeable changes in the UV−vis spectra (see Figure S8 for structures). First, **2d** has an initial peak at 512 nm, which is absent once the anchor atom is changed (Figure 5). Second, the

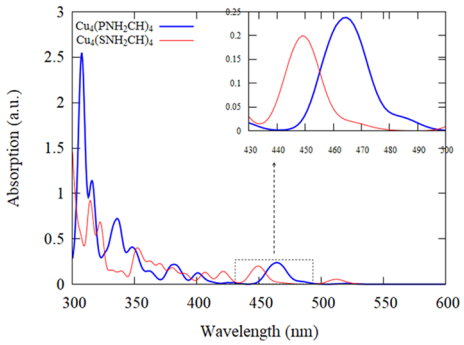

Figure 5. Theoretical UV−vis spectra of $Cu_4(PNH_2CH)_4$ and its anchor atom change to $Cu_4(SNH_2CH)_4$. The inset highlights the observed peaks between 430 and 500 nm.

first observable peak for **2c** resides at 465 nm and is a transition from HOMO − 1 to LUMO. This transition is similar for the peak at 449 nm in **2d**. Thus, change in the anchor atom from phosphorus to sulfur results in a hypochromic shift of the electronic transition from the HOMO − 1 to LUMO (Figure 5). The remaining spectra of **2c** and **2d** vary significantly. This may be due in part to electronic level rearrangement based on the change of the anchor atom that causes a large change in the geometry of the copper core as evidenced in Table 1.

Figure 6 provides a comparison of the electronic spectra for **1a**, **2a**, **3** (Cu_6), and **4** (Cu_{25}). The initial absorption peaks for Cu_6 and Cu_{25} reside between 700 and 1100 nm. While these are prominent peaks, these are bathochromic compared to the onset electronic transition in **1a** and **2a**. Interestingly, there are three transitions contributing to the initial peaks of systems **3** and **4**. In system **3**, the transitions occur between the HOMO → LUMO, HOMO − 3 → LUMO, and HOMO − 1 → LUMO. In system **4**, the transitions occur between the HOMO → LUMO, HOMO − 2 → LUMO, and HOMO − 1 → LUMO + 1. Interestingly, though the simulated spectra indicate that there may be some types of observable UV−vis peaks between 1100 and 700 nm, their oscillator strengths indicate that these may not be observable in the experimental spectra (Tables S5 and S6). For example, previous reports on the anion of **3** indicated that there was a discrepancy between the spectra obtained

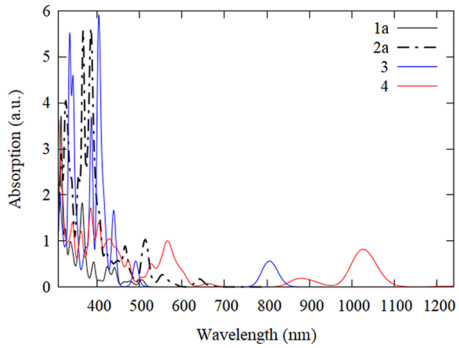

Figure 6. Theoretical UV−vis spectra of ligated copper systems **1a** ($Cu_4(SN_2C_7H_{11})_4$), **2a** ($Cu_4(PN(C_6H_5)_2CH)_4$), **3** ($Cu_6(SC_7H_4NO)_6$), and **4** ($Cu_{25}(SH)_{18}^-$).

theoretically and from experiment.[7] The discrepancy, i.e., experimentally unobserved optical peaks between 700 and 100 nm in theoretical spectra, can be explained by the low intensity found for the peak transitions. In general, the increased intensity observed around 400 nm (3.1 eV) for all systems is due to the involvement of ligand with the electron−hole pair (Supporting Information), while those transitions between 500 and 700 nm tend to involve more states mainly localized on the metal core.

It is interesting to ascertain how the systems calculated here compare to experimentally obtained spectroscopy data. A comparative analysis of the theoretically simulated optical absorption of **1a** was performed with previous experimental results for $Cu_4(SN_2C_7H_{11})_4$. Though the previously reported UV−vis spectrum is suggested to have the formula $[Cu(SN_2C_7H_{11})]_n$ (n = 1), the possibility of multiple species could be expected (Figure 7). Therefore, we also performed simulations on the $Cu(SN_2C_7H_{11})$ monomer as the previous report suggested that the species may be the monomer instead of

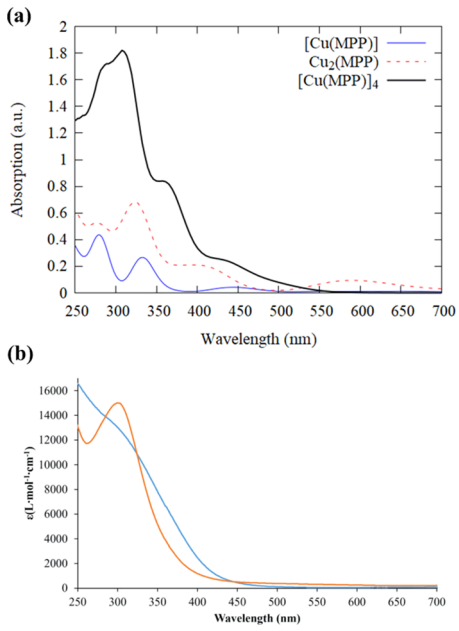

Figure 7. (a) Theoretical UV−vis of Cu(MPP) (blue line), Cu_2(MPP) (red, dashed line), and $[Cu(MPP)]_4$ (black, bold line), and (b) the UV−vis spectra of $[Cu(MPP)]_n$ (assuming n = 1) (orange line) and $Cu_2(MPP^*)_1$ (red, dashed line). (Reprinted with permission from ref 1. Copyright 2017 American Chemical Society.).

https://dx.doi.org/10.1021/acs.jpca.0c03992
J. Phys. Chem. A 2020, 124, 6504−6510

the $Cu_4(SR)_4$ species (Supporting Information). The UV−vis spectra obtained from the experiment shows one prominent peak around 300 nm. The simulated spectrum of the monomer has two prominent peaks at 330 and 270 nm (Figure 7a). On the other hand, the simulated spectrum at a Gaussian width of 0.15 of **1a** has a large prominent peak around 308 nm (Figure 7a). Interestingly, this prominent peak corresponds to transitions from deep-lying occupied molecular orbitals to nearly degenerate LUMO states, i.e., LUMO, LUMO + 3, and LUMO + 5. These results not only indicate that the experimental UV−vis spectrum is that of the $[Cu(SN_2C_7H_{11})]_4$ instead of the $[Cu(SN_2C_7H_{11})]$ monomer but also allow for the identification of the origin of transitions contributing to experimentally obtained spectroscopic data for atomically precise copper nanoclusters.

4. CONCLUSIONS

The theoretical investigation of geometry, electronic structure, and optical properties of closed-shell ligated copper nanoclusters were carried out using density functional theory and time-dependent density functional theory. Geometry optimizations for **1a**, **1b**, **1c**, **2a**, **2b**, **2c**, and **2d** were performed. The influence of the ligand on geometry, electronic structure, and optical properties was investigated. As one reduces the R-group on Cu_4 nanoclusters, the HOMO−LUMO gap increases by 0.15 eV on average. However, when the anchor atom from phosphorous to sulfur is changed, there is a large change in the gap from 2.02 to 2.34 eV. The large change is attributed to the bond lengths shortening significantly within the copper core. Based on the evaluation of the Kohn−Sham orbitals and charge analyses, we determined that nanoclusters have superatom shells.

A comparative analysis with two larger clusters, Cu_6 and Cu_{25}, was also performed to provide foundational insight about the variance of properties due to copper core size, which was lacking. Our results showed that as the size of the copper core increases, there was no observable trend in the Cu−Cu bond lengths, with fluctuations between 2.66 and 2.83 Å. However, as the copper core increases in size, the HOMO−LUMO gap decreases with **1b**/**c** having the largest HL gap (2.44 eV) and Cu_{25} the smallest (0.94 eV). The evolution in size of the copper core from $n = 4$ to $n = 25$ led to observable differences in the optical absorption spectra in part due to the change in electronic structure. The observable differences in the optical response due to size may be further enhanced or reduced through molecular interactions that may occur if these atomically precise nanoclusters are integrated into optical sensing devices. Further experimental and computational studies into the optical response variance of atomically precise copper nanoclusters at varying sizes due to (bio)-molecular interactions are warranted. Finally, through the comparison of theoretical and experimental spectra, our study illustrated how to discern the composition of the structures observed in the collected spectroscopic profile. These results not only fill a gap in the knowledge of atomically precise nanochemistry, but we hope this study encourages more investigations of ligated copper clusters for sensing devices.

■ ASSOCIATED CONTENT

Supporting Information

The Supporting Information is available free of charge at https://pubs.acs.org/doi/10.1021/acs.jpca.0c03992.

Relaxed structures for **1a-c**, **2a-d**, **3**, and **4**, bond averages and electron densities for HOMO and LUMO states of **1a**, **2a**, **3**, **4**, figures of theoretical optical spectra for **1a**, Cu(MPP), Cu_2(MPP), and **2a-c**, energies, oscillator strengths, electron−hole pair transitions and electron densities for selected peaks for **1a** and **2a** clusters, oscillator strengths and electron−hole pair transitions for Cu_6 and Cu_{25}, Information on the Hirschfield analysis and optical spectra in THF (PDF)

■ AUTHOR INFORMATION

Corresponding Author

Andre Z. Clayborne − *Department of Chemistry, Howard University, Washington, District of Columbia 20059, United States;* orcid.org/0000-0002-0574-0847; Email: andre.clayborne@howard.edu

Authors

Adebola Adeagbo − *Department of Chemistry, Howard University, Washington, District of Columbia 20059, United States;* orcid.org/0000-0002-4715-5013

Tao Wei − *Department of Chemical Engineering, Howard University, Washington, District of Columbia 20059, United States;* orcid.org/0000-0001-6888-1658

Complete contact information is available at: https://pubs.acs.org/10.1021/acs.jpca.0c03992

Author Contributions

The manuscript was written through the contributions of all authors. All authors have given approval to the final version of the manuscript.

Notes

The authors declare no competing financial interest.

■ ACKNOWLEDGMENTS

We thank Prof. Trevor Hayton for discussions about copper nanoclusters. The authors thank the support of the National Science Foundation (NSF 1831559). Prof. A.Z.C. thanks the National Natural Science Foundation of China (grant number 21750110448) for partial support. This work used the Extreme Science and Engineering Discovery Environment (XSEDE), which is supported by the National Science Foundation grant number ACI-1548562. Specifically, it used the Bridges system, which is supported by NSF award number ACI-1445606, at the Pittsburgh Supercomputing Center (PSC). Prof. T.W. thanks for computational resources to the Texas Advanced Computing Center (TACC).

■ REFERENCES

(1) Weerawardene, K. L. D. M.; Häkkinen, H.; Aikens, C. M. Connections Between Theory and Experiment for Gold and Silver Nanoclusters. *Annu. Rev. Phys. Chem.* **2018**, *69*, 205−229.

(2) Lopez-Acevedo, O.; Kacprzak, K. A.; Akola, J.; Häkkinen, H. Quantum Size Effects in Ambient CO Oxidation Catalysed by Ligand-Protected Gold Clusters. *Nat. Chem.* **2010**, *2*, 329−334.

(3) Zhao, J.; Jin, R. Heterogeneous Catalysis by Gold and Gold-Based Bimetal Nanoclusters. *Nano Today* **2018**, *18*, 86−102.

(4) Hu, M.; Chen, J.; Li, Z.-Y.; Au, L.; Hartland, G. V.; Li, X.; Marquez, M.; Xia, Y. Gold Nanostructures: Engineering Their Plasmonic Properties for Biomedical Applications. *Chem. Soc. Rev.* **2006**, *35*, 1084−1094.

(5) Sharma, S.; Chakrahari, K. K.; Saillard, J. Y.; Liu, C. W. Structurally Precise Dichalcogenolate-Protected Copper and Silver Superatomic Nanoclusters and Their Alloys. *Acc. Chem. Res.* **2018**, *51*, 2475−2483.
(6) Maity, S.; Bain, D.; Patra, A. Engineering Atomically Precise Copper Nanoclusters with Aggregation Induced Emission. *J. Phys. Chem. C* **2019**, *123*, 2506−2515.
(7) Gao, X. H.; He, S. J.; Zhang, C. M.; Du, C.; Chen, X.; Xing, W.; Chen, S. L.; Clayborne, A.; Chen, W. Single Crystal Sub-Nanometer Sized Cu6 (SR)6clusters: Structure, Photophysical Properties, and Electrochemical Sensing. *Adv. Sci.* **2016**, *3*, No. 1600126.
(8) Yuan, P.; Chen, R.; Zhang, X.; Chen, F.; Yan, J.; Sun, C.; Ou, D.; Peng, J.; Lin, S.; Tang, Z.; et al. Ether-Soluble Cu_{53} Nanoclusters as an Effective Precursor of High-Quality CuI Films for Optoelectronic Applications. *Angew. Chem., Int. Ed.* **2019**, *58*, 835−839.
(9) Chen, A.; Kang, X.; Jin, S.; Du, W.; Wang, S.; Zhu, M. Gram-Scale Preparation of Stable Hydride M@Cu_{24} (M = Au/Cu) Nanoclusters. *J. Phys. Chem. Lett.* **2019**, *10*, 6124−6128.
(10) Zall, C. M.; Linehan, J. C.; Appel, A. M. A Molecular Copper Catalyst for Hydrogenation of CO_2 to Formate. *ACS Catal.* **2015**, *5*, 5301−5305.
(11) Chakrahari, K. K.; Liao, J.-H.; Kahlal, S.; Liu, Y.-C.; Chiang, M.-H.; Saillard, J.-Y.; Liu, C. W. $[Cu_{13}\{S_2CNnBu_2\}_6(Acetylide)_4]^+$: A Two-Electron Superatom. *Angew. Chem., Int. Ed.* **2016**, *55*, 14704−14708.
(12) Wang, N.; Ga, L.; Ai, J. Synthesis of Novel Fluorescent Copper Nanomaterials and Their Application in Detection of Iodide Ions and Catalysis. *Anal. Methods* **2019**, *11*, 44−48.
(13) Kacprzak, K. A.; Lopez-Acevedo, O.; Häkkinen, H.; Grönbeck, H. Theoretical Characterization of Cyclic Thiolated Copper, Silver, and Gold Clusters. *J. Phys. Chem. C* **2010**, *114*, 13571−13576.
(14) Ghosh, A.; Huang, R.-W.; Alamer, B.; Abou-Hamad, E.; Hedhili, M. N.; Mohammed, O. F.; Bakr, O. M. $[Cu_{61}(StBu)_{26}S_6Cl_6H_{14}]^+$: A Core−Shell Superatom Nanocluster with a Quasi-J36 Cu_{19} Core and an "18-Crown-6" Metal-Sulfide-like Stabilizing Belt. *ACS Mater. Lett.* **2019**, *1*, 297−302.
(15) Sun, C.; Mammen, N.; Kaappa, S.; Yuan, P.; Deng, G.; Zhao, C.; Yan, J.; Malola, S.; Honkala, K.; Häkkinen, H.; et al. Atomically Precise, Thiolated Copper-Hydride Nanoclusters as Single-Site Hydrogenation Catalysts for Ketones in Mild Conditions. *ACS Nano* **2019**, *13*, 5975−5986.
(16) Han, B.-L.; Liu, Z.; Feng, L.; Wang, Z.; Gupta, R. K.; Aikens, C. M.; Tung, C.-H.; Sun, D. Polymorphism in Atomically Precise Cu23 Nanocluster Incorporating Tetrahedral [Cu4]0 Kernel. *J. Am. Chem. Soc.* **2020**, *142*, 5834−5841.
(17) Mortensen, J. J.; Hansen, L. B.; Jacobsen, K. W. Real-Space Grid Implementation of the Projector Augmented Wave Method. *Phys. Rev. B* **2005**, *71*, No. 35109.
(18) Enkovaara, J.; Rostgaard, C.; Mortensen, J. J.; Chen, J.; Dułak, M.; Ferrighi, L.; Gavnholt, J.; Glinsvad, C.; Haikola, V.; Hansen, H. A.; et al. Electronic Structure Calculations with GPAW: A Real-Space Implementation of the Projector Augmented-Wave Method. *J. Phys.: Condens. Matter* **2010**, *22*, No. 253202.
(19) Larsen, A. H.; Mortensen, J. J.; Blomqvist, J.; Castelli, I. E.; Christensen, R.; Dułak, M.; Friis, J.; Groves, M. N.; Hammer, B.; Hargus, C.; et al. The Atomic Simulation Environment—a Python Library for Working with Atoms. *J. Phys.: Condens. Matter* **2017**, *29*, No. 273002.
(20) Perdew, J. P.; Burke, K.; Ernzerhof, M. Generalized Gradient Approximation Made Simple. *Phys. Rev. Lett.* **1996**, *77*, 3865−3868.
(21) Nguyen, T.-A. D.; Cook, A. W.; Wu, G.; Hayton, T. W. Subnanometer-Sized Copper Clusters: A Critical Re-Evaluation of the Synthesis and Characterization of $Cu_8(MPP)_4$ (HMPP = 2-Mercapto-5-n-Propylpyrimidine). *Inorg. Chem.* **2017**, *56*, 8390−8396.
(22) Rathnayaka, S. C.; Lindeman, S. V.; Mankad, N. P. Multinuclear Cu(I) Clusters Featuring a New Triply Bridging Coordination Mode of Phosphaamidinate Ligands. *Inorg. Chem.* **2018**, *57*, 9439−9445.
(23) Akola, J.; Kacprzak, K. A.; Lopez-Acevedo, O.; Walter, M.; Grönbeck, H.; Häkkinen, H. Thiolate-Protected Au_{25} Superatoms as Building Blocks: Dimers and Crystals. *J. Phys. Chem. C* **2010**, *114*, 15986−15994.
(24) Walter, M.; Häkkinen, H.; Lehtovaara, L.; Puska, M.; Enkovaara, J.; Rostgaard, C.; Mortensen, J. J. Time-Dependent Density-Functional Theory in the Projector Augmented-Wave Method. *J. Chem. Phys.* **2008**, *128*, No. 244101.
(25) Pohjolainen, E.; Häkkinen, H.; Clayborne, A. The Role of the Anchor Atom in the Ligand of the Monolayer-Protected $Au_{25}(XR)_{18}^-$ Nanocluster. *J. Phys. Chem. C* **2015**, *119*, 9587−9594.
(26) Gao, X.; He, S.; Zhang, C.; Du, C.; Chen, X.; Xing, W.; Chen, S.; Clayborne, A.; Chen, W. Single Crystal Sub-Nanometer Sized $Cu_6(SR)_6$ Clusters: Structure, Photophysical Properties, and Electrochemical Sensing. *Adv. Sci.* **2016**, *3*, No. 1600126.
(27) Reveles, J. U.; Clayborne, P. A.; Reber, A. C.; Khanna, S. N.; Pradhan, K.; Sen, P.; Pederson, M. R. Designer Magnetic Superatoms. *Nat. Chem.* **2009**, *1*, 310−315.
(28) Häkkinen, H. Electronic Structure: Shell Structure and the Superatom Concept. In *Frontiers of Nanoscience*; Elsevier Science, 2015; Vol. *9*, pp 189−222.
(29) Clayborne, P. A.; Lopez-Acevedo, O.; Whetten, R. L.; Grnbeck, H.; Hkkinen, H. Evidence of Superatom Electronic Shells in Ligand-Stabilized Aluminum Clusters. *J. Chem. Phys.* **2011**, *135*, No. 094701.
(30) Lopez-Acevedo, O.; Clayborne, P. A.; Häkkinen, H. Electronic Structure of Gold, Aluminum, and Gallium Superatom Complexes. *Phys. Rev. B: Condens. Matter Mater. Phys.* **2011**, *84*, No. 035434.
(31) Hirshfeld, F. L. Bonded-Atom Fragments for Describing Molecular Charge Densities. *Theor. Chim. Acta* **1977**, *44*, 129−138.

https://dx.doi.org/10.1021/acs.jpca.0c03992
J. Phys. Chem. A 2020, 124, 6504−6510